# Characteristics of neutralization process of acid mine drainage with steel slag

**Lei Yang** ( fivsix526@gmail.com )
China University of Mining and Technology
**Yuegang Tang**
China University of Mining and Technology
**Mingyuan Yang**
Chongqing University of Technology
**Duanning Cao**
Chongqing University of Technology
**Cunfang Lu**
Chongqing University of Technology
**Yuanyuan He**
Chongqing University of Technology

**Research Article**

**Keywords:** acid mine drainage, basic oxygen furnace, steel slag, acid neutralization capacity, alkaline, gypsum.

**Posted Date:** March 24th, 2022

**DOI:** https://doi.org/10.21203/rs.3.rs-1413630/v1

# Abstract

Steel slag has been proven to be an effective environment remediation media for acid neutralization, and a potential aid to mitigate acid mine drainage (AMD) in passive treatment process. In application, the acid neutralization capacity (ANC) of the steel slag is often decreased after a period of use because of the precipitate formation. However, the characteristic of the formation process are unclear yet. In this work, we tested the ANC of the commonly used Basic Oxygen Furnace (BOF) steel slag by titration of simulated AMD ($H_2SO_4$, 0.1M) and real AMD from abandoned coal mine drainage in the southwestern of China. The result indicated that there was a linear relationship between pH value and titrated AMD amount, for both simulated AMD and real AMD. When the pH decreased to 7, the titrated AMD amount and ANC were about 40ml and 8mmol $H^+$/g slag for simulated AMD. At the beginning of the titration process, dissolution and hydration reactions of the easily dissolved calcium-containing constitute played a dominant role, and then were the precipitation formation reactions. The turning point for the two reactions was occurred when 20 % of the total titrated amount was titrated. Meanwhile, the BOF slag surface became smooth, and the dissolution reactions were hindered when the slag surface was clogged by the new formed crystallized gypsum. Further titration experiments results by real AMD also confirmed the ANC variation of BOF samples during the neutralization process.


# 1 Introduction

Steel slags are a category of alkaline industrial waste produced in steel making process. The crude steel output from China was 1053.3 million tons in 2020, accounting for 56.7% of the whole world (Yang et al. 2021). The amount of steel slag produced in 2020 was 158 million ton according to the ratio that there were 150 Kg steel slags produced per ton of crude steel (Mohammed and Yaacob 2016, Feng et al. 2004, Zhang et al. 2020). As the largest crude steel production country, China's steel slag utilization ratio was only 30%, it is lower than that of the development countries, shown in Table 1.

Table 1
Utilization ratio of steel slag in different countries (%)

| | Inner recycling | Road | Cement | Construction | Temporary storage | Others | Unutilized | Reference |
|---|---|---|---|---|---|---|---|---|
| Japan | 20.8 | 32.4 | 3.4 | 34.8 | - | 7 | 1.6 | |
| USA | - | 49.7 | 3.3 | 16 | - | 15.4 | 15.6 | |
| China | 7.4 | 7.6 | 10.3 | - | - | 4.7 | 70 | |
| Europe | 11 | 43 | 5 | 6 | 19 | 3 | 13 | |

Nowadays the most common utilization patterns include road project construction, cement production, plant recycling and et al. (Saha et al. 2019, Yang et al. 2021). Although many efforts were made to increase the steel slag recycling ratio in the construction materials, however, the performance of the produced construction materials was frequently substandard (Zvimba et al. 2017), because the free CaO, MgO and other easily hydrated components in steel slag could deteriorate the cement stability associated with the volume stability of the products (Zhang et al. 2020, Yu et al. 2015). It was reported that the acceptable contents of f-CaO and MgO should be lower than 7% and 4% when the steel slags were used in unbound and bitumen bound layers (Zhang et al. 2020). Therefore, it is necessary to explore new ways to increase the utilization ratio of steel slags, such as the soil remediation (Sheng,

Huang et al. 2014), metal adsorption (Tabelin et al. 2020, Sithole et al. 2020, Zhan et al. 2019, Asere et al. 2019), AMD neutralization (Zvimba et al. 2017, Saha et al. 2019)and other pollution control applications.

When steel slag was applied at the AMD neutralization process, the acidity of the drainage could be neutralized by the alkaline components of steel slag, like dicalcium silicate ($C_2S$), tricalcium silicate ($C_3S$), free calcium oxide (f-CaO), free magnesium oxide (MgO) and et al. (Kruse et al. 2012). Previous researches confirmed that the steel slags are more excellent in alkaline production than the traditional materials, such as lime stone (Molahid et al. 2019), lime, soda alkaline and dolomite (Sukati et al. 2018). The alkalinity concentrations of limestone leach bed were around 5 mg/L $CaCO_3$/L, with maximums concentration at around 80 mg/L $CaCO_3$/L, whereas they are usually above 100 mg/L $CaCO_3$/ L for steel slag leach beds (SSLB) (Goetz and Riefler 2014a, Kruse et al. 2012). Besides, the neutralization ability of lime will become worse with the increase of treatment time, while the maximum alkaline concentrations of steel slag could reach 2000 mg/L $CaCO_3$/L even after many years of service (Wang and Yan 2010, Goetz and Riefler 2014b, Kruse et al. 2012).

The running results of steel slag leach beds (SLB) indicated that its performance was influenced by many factors, including the effluent quality (Goetz and Riefler 2014b), slag alkalinity loadings (Name and Sheridan 2014), slag particle size distribution (Alizadeh and Naseri 2014) and et al.. Comparing the treatment results of SLBs built for one year and historical data of previous years, it was found that the precipitates in the effluent piping and within the slags reduced the ANC of the slag, and the effluent pH value was lower than the designed value (Tabelin et al. 2020, Goetz and Riefler 2014b). To meet the AMD emission standards, it is necessary to replace the slags in SLB before the effluent was substandard. Therefore, it is significant to clarify the steel slags characteristics during the AMD neutralization process.

In the present study, the variation of slag properties, including acid neutralization capacity (ANC), leaching behavior and the micromorphology during the neutralization process were systematically investigated. SLB treatment process was simulated by titration experiments with simulated AMD and real AMD. The experiment results were aim to explain the precipitate formation mechanism, and to provide fundamental guide for SLB operations.

## 2 Materials And Methods

# 2.1 Steel slag sampling

The basic oxygen furnace (BOF) steel slag samples used in the present study were obtained from Shougang Group Shuicheng Steel Company, Guizhou Province, China. The fresh slags were sampled after crushing, drying overnight at 105°C and screening through sieves of 20 mesh, 50 mesh, 100mesh and 200 mesh before used.

# 2.2 Material Characterization

Compositions of the BOF steel slag samples were quantitatively analyzed by X-ray fluorescence (XRF) using an XRF-1800 Analyzer (Shimadzu Corp., Kyoto, Japan). The phase compositions were performed by Powder X-ray diffraction (XRD) using a Smartlab X-ray diffractometer (Rigaku Corp., Tokyo, Japan) with the operating parameters of Cu Kα radiation (λ = 1.5418 Å) and 40 kV/200 mA power generator. An angular range of 0 − 90° 2θ was measured with a step size of 0.02° and a 1 s counting time per step. The identifications of all crystalline phases were undertaken with JADE6 software (Materials Data, Inc., Livermore, CA, USA) and the PDF-2 2004 database (International Centre for Diffraction Data, Newton Square, PA, USA). The morphology of the BOF steel samples was observed using a scanning electron microscopy (SEM) (Zeiss, Oberkochen, Germany). All slags

samples were sputtered coated with an approximately 5 nm-thick layer of carbon before observation. The concentrations of elements Ca, Mg, Si, Al, Mn, Fe and Cr in solutions were determined by inductively coupled plasma (PerkinElmer Avio 500).

## 2.3 Alkalinity releasing property of steel slag

To know the releasing properties of slag samples, alkalinity of the leached solutions were determined according to the acid titration method SL83-1994 China. The leached solution was prepared by taking 1.0g steel slag into 100mL DI water with a rotating speed of 100r/min for various set time. When reached the set time, the mixtures were separated by filtration of a 0.45 μm filter (Merck). Then the pH and alkalinity of the collected filtrate were determined, the alkalinity was calculated and expressed as calcium carbonate ($CaCO_3$).

## 2.4 Steel slag ANC determination procedure

The ANC solution was prepared firstly by adding 1.0 g slag to 100 ml DI water and stirred at 500 rpm for 4 h; then adding the simulated AMD (0.1 mol/L $H_2SO_4$) and real AMD into the ANC solution by drop pipette at the rate of 1–2 ml one titration. The pH of the solution was determined once after titration procedure. It was found that, before the next titration, the pH had a re-rise because the alkaline components in steel slag could neutralize the titrated simulated AMD in solution. With the amount of the AMD amount increasing, the alkaline components in slag would be exhausted, and the endpoint was reached. The titration endpoint was regulated that at the time when the re-rise value of pH was less than 0.05 after titration. After reaching the endpoint, the mixture were separated by filtration of a 0.45 μm filter (Merck) and preserved in pre-cleaned polypropylene bottles. As previously described, the filter liquor and residue were determined by ICP, XRD, SEM, respectively.

## 2.5 Leaching ratio

To investigate the slag leach ability during the titration process, leaching ratios of element in slag samples were calculated according to formula (1).

$$r = \frac{c_1 \bullet V}{c_2 \bullet m}$$

1

Where, $r$ is the leaching ratio for specific element; $c_1$ is the concentration in filter liquor; $V$ is the filter liquor volume; $c_2$ is the mass percentage in slag samples; $m$ is the mass of the slag samples.

# 3 Results Experiment

### 3.1 Chemical characteristic of raw steel slags.

Table 2 Compositions of steel slag sample (%)

| Composition | CaO | $Fe_2O_3$ | $SiO_2$ | MgO | MnO | $Al_2O_3$ | $P_2O_5$ | $V_2O_5$ | $Cr_2O_3$ |
|---|---|---|---|---|---|---|---|---|---|
| Content | 41.82 | 25.05 | 11.89 | 6.61 | 5.48 | 2.18 | 1.59 | 0.73 | 0.69 |

The main chemical compositions of the BOF steel slag were shown in Table 2. Except for the listed components in Table 2, there were some coexisted minor constituents in the slag samples, like ZnO, SrO, $MoO_3$, KO, CuO. These

substance proportions were very small and made negligible contribution to the ANC of steel slag, therefore, only the main components concentrations of Ca, Fe, Si, Mg, Al, Cr and Mn in the filter liquor were determined, other minor components were not considered in the study.

The XRD components of steel slag sample were shown in Fig.1 (a). It is known the slags are heterogeneous materials consisting of a mixture of crystalline phases. The analysis of the diffraction lines revealed that the major constituent phases in steel slag matrix were $Ca_2SiO_4$ (calcium silicate), $Ca_3SiO_5$ (tricalcium silicate), $CaFe_2O_4$ (calcium ferrite)CaO (lime) and RO phase, however, the f-CaO diffraction peak was not prominent.

The SEM image of slag samples and the magnified SEM image were shown in Fig 1(b) and Fig. 1(c). It can be seen that the slag particles had a loose amorphous microstructure.

The alkalinity releasing results of slag samples were shown in Fig. 1(d). The alkalinity concentration was close to stable after 60 min. For the mentioned L/S ratio (1:100), the stable alkalinity was in a range of 100-110 mg/L and the corresponding pH of the filtrate was 10.5.

Calcium containing components in BOF slags were mainly originated from flux materials during the steel making process, like lime, limestone. (Zvimba et al. 2017). The unreacted limestone was transformed to free CaO and was left in slag, while the reacted lime stone were transfer to dicalcium silicate ($C_2S$) and tricalcium silicate ($C_3S$), and calcium ferrite et al. (Manchisi et al. 2020). For this reason, the percentage of the free CaO in slags was limited. Therefore, the f-CaO diffraction peak in XRD was not prominent in this sample. The alkalinity releasing tests results verified that the alkalinity concentrations in solution was abundant, which was in consistence with observation in the previous study (Goetz and Riefler 2014a). Meanwhile, the enlarged SEM image confirmed the loose amorphous microstructure of slag, which had positive influence on the metal removal by providing big surface area and inner channels (Yang et al. 2021).

### 3.2 Steel slag ANC determination

The ANC results titrated by simulated AMD was shown in Figure 2 (a). With the simulated AMD amount increasing, the pH value of the solution decreased to 2.15 gradually. When reaching the endpoint, the total titrated simulate AMD amount was 115ml for 1 g slag. And it was about 40 ml when the pH decreased to the neutral rang 7.07. The relationship between pH and simulated AMD amount was basically with the linear law in the whole process, the square R was 0.94. To know the influence of particle size on the ANC, slag samples of 20, 50 and 100 mesh were also titrated shown in Fig. 2 (b). The results indicated that the particles size of the slag had significant influence on the ANC. The total titrated amounts of simulated AMD were 8 ml, 14 ml and 45 ml for steel slag particles of 20, 50 and 100 mesh. It means the ANC increased dramatically when the particle size became small. Particles size distribution was an important designed parameter in practice. The recommended size of slag was less than 3mm in SLB (Alizadeh and Naseri 2014). However, the fine particle slags in SLB were more likely to precipitate on the bottom of the beds, and to increase the running resistance (Alizadeh and Naseri 2014 , Iakovleva et al. 2015), especially for the passive treatment applications. Therefore, for slag applications, it is necessary to optimize the steel slag particle size distribution according to the ANC demand and the geographical environment of remediation site, so as to balance the advantages and disadvantages of the fine particle size.

### 3.3 Slag leaching behavior characteristics

It was reported that the f-CaO and other Ca-containing components in BOF slag samples would react with acid firstly, because they are easily dissolved in acidic solution (Mulopo et al. 2012). But the dissolution behaviors of other components in samples were unknown yet. Based on the ANC results, the intermediate process of the titration were sample when the accumulative amount were 20 %, 40%, 60% and 80% of the total amount at the endpoint, i.e. the intermediate amount were 23ml, 46ml, 68ml and 92ml. The procedure was consistence with the ANC determination mentioned above. The experimental results were shown in Fig. 3. It was found that the leaching ratios of all the tested elements in solution were increased with the AMD amount increasing, but each element exhibited distinctive characteristics.

Ca content in the slag was 41.82 % calculated as oxide. In leaching results, its leaching ratio was increased firstly and then decreased. The maximum value was 28.73 % when the titration amount was 46mL, and the corresponding concentration was 9.20 mg/l. Both concentration curves and leaching ratio curves had similar variation trends.

For Mg and Mn containing constitutes, their concentrations in solution increased directly with the increase of the titrated simulated AMD amount. Mg had the maximum leaching ratio of 56.75 %. However, the percentages of MgO and MnO in steel slag were relatively few. At the titration endpoint, the final concentrations of element Mg and Mn in solution were 2.03 mg/l and 0.06 mg/l, which had minor influence on the the slag alkalinity.

For elements Al, Fe and Cr, the leaching ratios were close to zero till the titrated AMD was more than 69 ml, particularly for Al and Fe. The pH variation result in Fig. 3 indicated that for the solution titrated 60 ml simulated AMD, the solution pH was 7. In other words, when the titrated AMD amount was less than 60 ml, the solution was alkaline. Thus, Al and Fe were likely to precipitate as hydroxide in alkaline solution. Elements concentration in Fig. 3(b) also showed that the concentration of Al, Fe, and Cr were very 0.31 mg/l, 2.14 mg/l and 1.06 mg/l at the endpoint.

# 4. Mechanism Discussion

### 4.1 Component phase variation

The interaction of these components with the AMD changes the steel slag characteristics and causes the phase transformation. Fig. 4 showed the phase transformation of slag samples characterized by XRD during the simulated AMD titration process. It can be seen that the diffraction intensity of the titrated steel slag was much higher than of the raw steel slag in Fig. 1 (a). It may be caused by the removal of the amorphous materials when the sample was washed by DI water and simulated AMD. For the steel slag sample titrated by 23 mL simulated AMD, the diffraction intensity of $C_2S$, $C_3S$ and RO were weaker than of the raw steel slag. Meanwhile, the gypsum diffraction peaks were emerged. For the steel slag samples adding 46 mL and 69mL simulated AMD, the diffraction intensity of the gypsum became stronger. For the sample titrated 115 mL simulated AMD, only gypsum diffraction peaks were present in the XRD pattern result.

As mentioned above, the steel slag was a complicated heterogeneous solid mixture produced in a molten state at high temperature and cooled down by various process (Sithole et al. 2020). According to the dissolution amount, the alkaline components in steel slag could be classified into three groups, the first group were f-CaO, MgO, calcium ferrite and dicalcium ferrite ($2CaO{\cdot}Fe_2O_3$); the second group included weakly bound CaO, MgO and some loosed bound $C_2S$; while the third group contained some tightly bound lime ($C_3S$、$C_2S$, MgO and wustite (FeO)) (Bodurtha

and Brassard 2000). Gibbs free energy of the reactions showed that the reaction sequence of components with simulated AMD were CaO, MgO, FeO, $C_2S$, $C_2F$, $C_3S$ under room temperature. It means that the dissolved CaO, MgO and FeO had priority to react with simulated AMD over $C_2S$, $C_3F_2$ and $C_3S$. (Manchisi et al. 2020, Bodurtha and Brassard 2000, Xue et al. 2013). The dissolution and hydration reaction occurred in the titration process were listed in Table 3.

Table 3 The reactions in the titration process

| Composition | Reaction equations |
|---|---|
| CaO | $CaO + 2H^+ \rightarrow Ca^{2+} + H_2O$ |
| MgO | $MgO + 2H^+ \rightarrow Mg^{2+} + H_2O$ |
| $Ca(OH)_2$ | $Ca(OH)_2 + 2H^+ \rightarrow Ca^{2+} + 2H_2O$ |
| $Mg(OH)_2$ | $Mg(OH)_2 + 2H^+ \rightarrow Mg^{2+} + 2H_2O$ |
| $Ca_2SiO_4$ | $Ca_2SiO_4 \rightarrow 2CaO + SiO_2$ |
| | $2CaO + 4H^+ \rightarrow 2Ca^{2+} + 2H_2O$ |
| $Ca_3SiO_6$ | $Ca_3SiO_6 \rightarrow 3CaO + SiO_2$ |
| | $3CaO + 6H^+ \rightarrow 3Ca^{2+} + 3H_2O$ |
| $Ca_2Fe_2O_5$ | $Ca_2Fe_2O_5 \rightarrow 2CaO + Fe_2O_3$ |
| | $3CaO + 6H^+ \rightarrow 3Ca^{2+} + 3H_2O$ |
| $CaSO_4$ | $Ca^{2+} + SO_4^{2-} \rightarrow CaSO_4$ |

Slag components transformation process could be speculated according to the leaching results and XRD results. The overall reaction process between AMD and slag samples could be divided into dissolution stage and precipitate stage. In the dissolution stage, the f-CaO, MgO and some loosed bound CaO would be released into the solution and hydrated with the acidic component in AMD, resulting in the rise of calcium concentration and leaching ratios, and the weakness of $C_2S$ and $C_2F$ peaks in XRD results. While in the precipitate stage, the hydrated calcium ions would react with the sulfate anions in AMD and form gypsum, leading the decrease of the calcium concentration and leaching ratios, and the immergence and growth of gypsum peaks in XRD results. The titration amount of 46 ml, i.e. the 40 % of the endpoint was a turning point of the two stages.

### 4.2 The morphology transformation

To further observe the phase transformation during the titration procedure, the microstructure and morphology of the sample particles were determined by SEM.

It can be seen that the majority ingredients of the slag samples were in circular shape from SEM images Fig. 5 (a) and (b). They had similar morphology as the raw samples in Fig.1. The two samples contained few large plate particles with a diameter of about 15μm. But for samples treated by 46 mL, 92 mL and 115 mL simulated AMD in Fig. 5 (c) , (d) and (e), the majority components of the slags were long crystallized trips with a length of 10-20 μm. With the titration amount increasing, the crystal size of gypsum became bigger and surface became smoother. What is more, the SEM image results were also confirmed the turning point of dissolution step and precipitate step speculation mentioned above.

### 4.3 AMD neutralization mechanism discussion

The detail of the neutralization process between steel slag and simulated AMD could be concluded as in Fig.6. (I) Slag component, such as f-CaO, MgO, $CaO{\cdot}Fe_2O_3$, loosed bound $C_2S$ on the surface of the samples particles are easily dissolved and they reacted with AMD firstly; (II) With the simulated AMD addition increasing, the titrated AMD transferred to the inner channel of the slag particles, and react with the alkaline substance in steel slag; (III) With the acid amount further increasing, some tightly bound $C_2S$ and few $C_3S$ in steel slag were decomposed releasing the calcium containing substance, simultaneously new formed gypsum were precipitated on the surface of the slag particles. With the gypsum precipitation going on, the inner pores of the steel slag particles were blocked and the alkaline releasing behaviors were gradually stopped. External coating, armors of iron hydroxides were also found when AMD was neutralized by lime in the passive treatment (Skousen et al. 2019 , Manchisi et al. 2020). The formation process was similar to the gypsum in the present study.

## 5. Slag Anc Confirmation Test By Real Amd

To investigate the ANC property of the slag samples in application, real AMD (pH = 2.35) from an abandoned coal mine in Guizhou Province China was used. Composition of the real AMD was shown in Table 4.

Table 4
Composition of real AMD with titration (mg/L)

| Composition | Na | Mg | Al | K | Ca | Mn | Fe | Co | Ni | Zn | $SO_4^{2-}$ |
|---|---|---|---|---|---|---|---|---|---|---|---|
| Content | 67.34 | 123.13 | 43.16 | 9.80 | 85.35 | 1.56 | 495.82 | 0.32 | 0.42 | 1.17 | 2689.96 |

Titration procedure was consistence with that of the simulated AMD, the obtained pH variation trend with the real AMD amount was described in Fig. 7. The results indicated that the total titrated real AMD amount was 670 mL for 1g slag sample, and there was a linear relationship between pH and real AMD amount with the square R 0.92, shown in Fig. 7 (a). When the pH reached the neutral vale (pH was 7), the titrated amount of real AMD was about 230 ml.

For BOF samples in the present study, the calculated ANC were about 8mmol $H^+$/g slag when the pH decreased to 7. EAF steel slag was titrated by similar method using $HNO_3$ (1M) as simulated AMD. When the solution pH decreased to 7, the calculated ANC of EAF was about 5.5 mmol $H^+$/g slag and 7.5 mmol $H^+$/g slag for short and long experiments (Jinying Yan 2000). Therefore, the experiments results were basically consistence considering the difference of slag composition, ion strength of the simulated AMD. But, for the real AMD titration experiment, the final ANC results was only 0.85 mmol $H^+$/g slag and 2.34 mmol $H^+$/g slag when the pH decreased to 7 and the endpoint. So there was a big gap between the simulated AMD results and the simulated AMD, which may be

caused by the reactions between metal ions in real AMD and the hydrated OH-, like $Mg^{2+}$, $Al^{3+}$, $Fe^{2+}$ et.al. These metal ions would consume some alkaline components in real AMD and decreased the ANC value (Sephton and Webb 2019, Tabelin et al. 2020). Further to determine the formation of the metal caused precipitate, element distribution on samples surface titrated by real AMD was determined by EDS. The results were shown in Fig. 7 (b). As can be seen, components containing Ca, S, Mg, Si, Al and Fe were obvious on the surface of the slag sample. Among them, the calcium enrichment areas were the same as that of element S, it can be speculated there gypsum formation as described of the simulated AMD sample. Fe, Si and Mg enrichment on the surface was also evident, but at different areas from Ca and S.

# 6. Conclusions

AMD neutralization remediation by steel slag could make full use of the alkaline substances in steel slag. With the dissolution of slag proceeding, calcium and magnesium concentration in solution increased. The maximum leaching ratio of Ca was 28.73% when 20% of the endpoint amount simulated AMD used. It can be considered as the turning point of dissolution stage and precipitate stage. The produced crystallized gypsum on the surface of slag was smooth and clean, which prevented the dissolution of the inner constitutes in slag. The ANC results indicated that there was a linear relationship between pH variation and AMD amount for both simulated and real AMD. When the pH decreased to 7, the calculated ANCs were 8 mmol $H^+$/g slag and 0.85 mmol $H^+$/g slag for simulated AMD and real AMD, respectively. In addition, the particle size distribution had significant influence on the ANC property of slag. Therefore, the utilization ratio of alkaline substances in steel slag was not high, especially for large particles employed in the AMD treatment application. To further improve the alkaline substance usage rate, the precipitate process on the surface of slag should be arrested and investigated in future investigation.

# Declarations


### Acknowledgments

The authors are grateful for the financial support provided by the Project of Guizhou science and Technology Department (No. 20204Y007), Science and Technology Research Program of Chongqing Municipal Education Commission (KJQN201801126).


**Author contribution** L. Yang: Conceptualization, Investigation, Methodology, Formal analysis, Validation, Writing - Original draft; Y. Tang: Project administration, Resources, Supervision, Writing -review & editing; M. Yang: Resources, Formal analysis; D. Cao: Data verification, Visualization; C. Lu: Resources, Supervision, Writing -review & editing; Y. He: Supervision, Writing -review & editing;

**Data availability** All data generated or analysed during this study are included in this published article [and its supplementary information files].

**Ethics approval and consent to participate** Not applicable.

**Consent for publication** Not applicable.

**Competing interests** The authors declare no competing interests.

# References

1. Alizadeh, Naseri (2014) An Investigation on the Influence of EAF Slag Particle Size on AMD Neutralization Behavior in Static and Dynamic Slag Leaching Systems. Mine Water and the Environment, 34: 204–212.https://doi:10.1007/s10230-014-0302-8
2. Asere, Stevens, Du Laing (2019) Use of (modified) natural adsorbents for arsenic remediation: A review. Sci Total Environ, 676: 706–720.https://doi:10.1016/j.scitotenv.2019.04.237
3. Bodurtha, Brassard (2000) Neutralization of Acid by Steel-Making Slags. Environmental Technology, 21: 1271–1281.https://doi:10.1080/09593332108618151
4. Feng, Van Deventer, Aldrich (2004) Removal of pollutants from acid mine wastewater using metallurgical by-product slags. Separation and Purification Technology, 40: 61–67.https://doi:10.1016/j.seppur.2004.01.003
5. Goetz, Riefler (2014a) Geochemistry of CO2 in Steel Slag Leach Beds. Mine Water and the Environment, 34: 42–49.https://doi:10.1007/s10230-014-0290-8
6. Goetz, Riefler (2014b) Performance of steel slag leach beds in acid mine drainage treatment. Chemical Engineering Journal, 240: 579–588.https://doi:10.1016/j.cej.2013.10.080
7. Iakovleva, Mäkilä, Salonen, et al. (2015) Acid mine drainage (AMD vs unmodified and modified limestone. Ecological Engineering, 81: 30–40.https://doi:10.1016/j.ecoleng.2015.04.046
8. Jinying Yan (2000) The long-term acid neutralizing capacity of steel slag. WASTE MANAGEMENT, 20: 217–223.https://doi:DOI: 10.1016/s0956-053x(99)00318-9
9. Kruse, Mackey, Bowman, et al. (2012) Alkalinity production as an indicator of failure in steel slag leach beds treating acid mine drainage. Environmental Earth Sciences, 67: 1389–1395.https://doi:10.1007/s12665-012-1583-5
10. Manchisi, Matinde, Rowson, et al. (2020) Ironmaking and Steelmaking Slags as Sustainable Adsorbents for Industrial Effluents and Wastewater Treatment: A Critical Review of Properties, Performance, Challenges and Opportunities. Sustainability, 12: 2118.https://doi:10.3390/su12052118
11. Mohammed, Yaacob (2016) Remediation of AMD using industrial waste adsorbents. AIP Conference, 1784: 060043.https://doi:10.1063/1.4966881
12. Molahid, Mohd Kusin, Madzin (2019) Role of multiple substrates (spent mushroom compost, ochre, steel slag, and limestone) in passive remediation of metal-containing acid mine drainage. Environ Technol, 40: 1323–1336.https://doi:10.1080/09593330.2017.1422546
13. Mulopo, Mashego, Zvimba (2012) Recovery of calcium carbonate from steelmaking slag and utilization for acid mine drainage pre-treatment. Water Sci Technol, 65: 2236–2241.https://doi:10.2166/wst.2012.143
14. Name, Sheridan (2014) Remediation of acid mine drainage using metallurgical slags. Minerals Engineering, 64: 15–22.https://doi:10.1016/j.mineng.2014.03.024
15. Saha, Sarkar, Sinha (2019) Use of Basic Oxygen Furnace (BOF) Steel Slag for Acid Mine Drainage Treatment: A Laboratory Study. Mine Water and the Environment, 38: 517–527.https://doi:10.1007/s10230-019-00615-3
16. Sephton, Webb (2019) The role of secondary minerals in remediation of acid mine drainage by Portland cement. J Hazard Mater, 367: 267–276.https://doi:10.1016/j.jhazmat.2018.12.035
17. Sithole, Ntuli, Okonta (2020) Fixed bed column studies for decontamination of acidic mineral effluent using porous fly ash-basic oxygen furnace slag based geopolymers. Minerals Engineering, 154: 106397.https://doi:10.1016/j.mineng.2020.106397
18. Skousen, Ziemkiewicz, Mcdonald (2019) Acid mine drainage formation, control and treatment: Approaches and strategies. The Extractive Industries and Society, 6: 241–249.https://doi:10.1016/j.exis.2018.09.008

19. Sukati, De Jager, Annandale, et al. (2018) The Hazardous Status of High Density Sludge from Acid Mine Drainage Neutralization. Sustainability, 10: 4185.https://doi:10.3390/su10114185
20. Tabelin, Corpuz, Igarashi, et al. (2020) Acid mine drainage formation and arsenic mobility under strongly acidic conditions: Importance of soluble phases, iron oxyhydroxides/oxides and nature of oxidation layer on pyrite. J Hazard Mater, 399: 122844.https://doi:10.1016/j.jhazmat.2020.122844
21. Wang, Yan (2010) Hydration properties of basic oxygen furnace steel slag. Construction and Building Materials, 24: 1134–1140.https://doi:10.1016/j.conbuildmat.2009.12.028
22. Xue, Wu, Zhou (2013) Adsorption characterization of Cu(II) from aqueous solution onto basic oxygen furnace slag. Chemical Engineering Journal, 231: 355–364.https://doi:10.1016/j.cej.2013.07.045
23. Yang, Lu, Quan, et al. (2021) Mechanism of Acid Mine Drainage Remediation with Steel Slag: A Review. ACS Omega.https://doi:10.1021/acsomega.1c03504
24. Yu, Liang, Wang, et al. (2015) Phosphate removal from domestic wastewater using thermally modified steel slag. J Environ Sci (China), 31: 81–88.https://doi:10.1016/j.jes.2014.12.007
25. Zhan, Xiao, Liang (2019) Removal of Pb(II) from Acid Mine Drainage with Bentonite-Steel Slag Composite Particles. Sustainability, 11: 4476.https://doi:10.3390/su11164476
26. Zhang, Chen, Jiang, et al. (2020) The potential utilization of slag generated from iron- and steelmaking industries: a review. Environment Geochem Health, 42: 1321–1334.https://doi:10.1007/s10653-019-00419-y
27. Zvimba, Siyakatshana, Mathye (2017) Passive neutralization of acid mine drainage using basic oxygen furnace slag as neutralization material: experimental and modelling. Water Sci Technol, 75: 1014–1024.https://doi:10.2166/wst.2016.579

# Figures

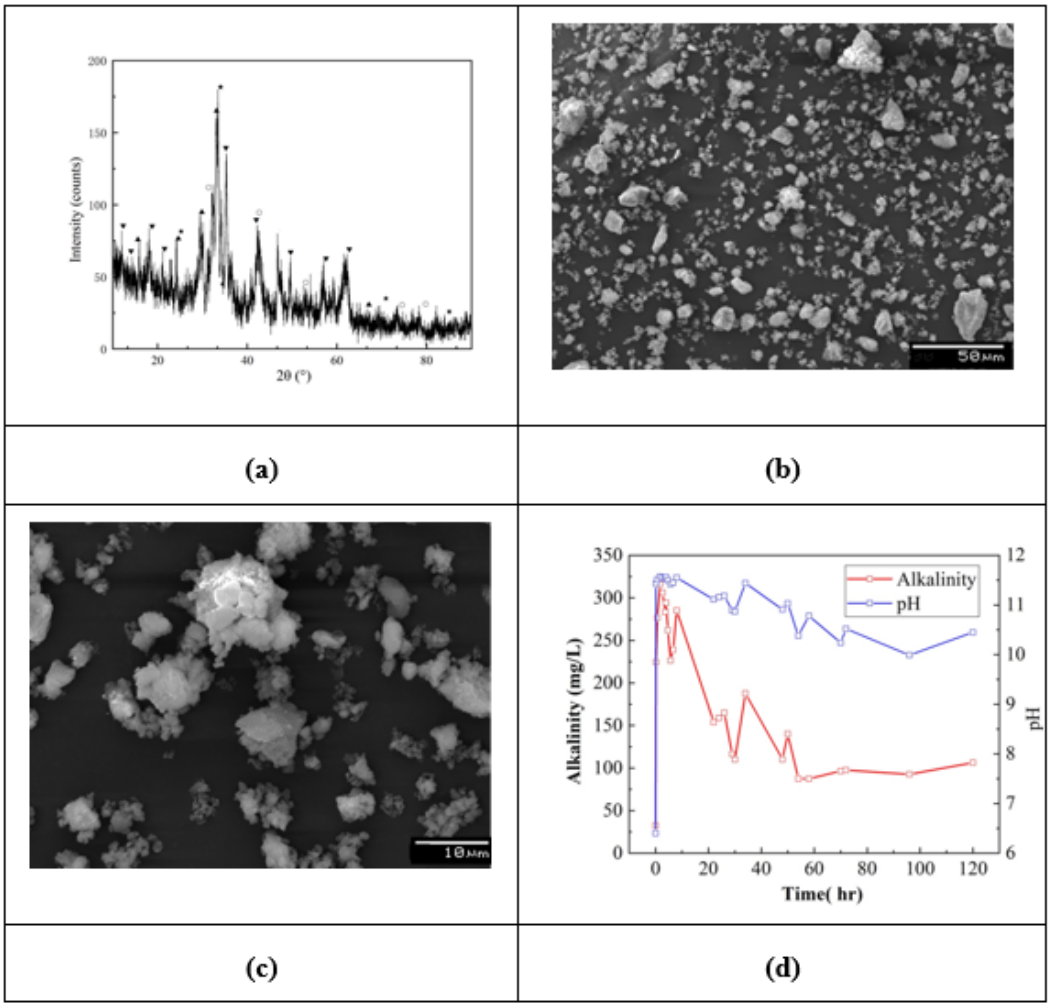


## Figure 1

Characterization results of the raw slag sample. (a) XRD patterns of steel sample, (● ) Hedenbergite, $CaFeSi_2O_6$; (▲) Mg-Al hydrotalcite; (▯)lime, CaO; (▼) Calcium silicate, $Ca_2SiO_4$; (▯) RO, $(Mg, Mn, Ca)_x Fe_{1-x}O$, (□) Tricalcium silicate, $Ca_3SiO_5$; (b)  SEM image; (c) enlarged SEM image; (d) alkalinity and pH variation with time.

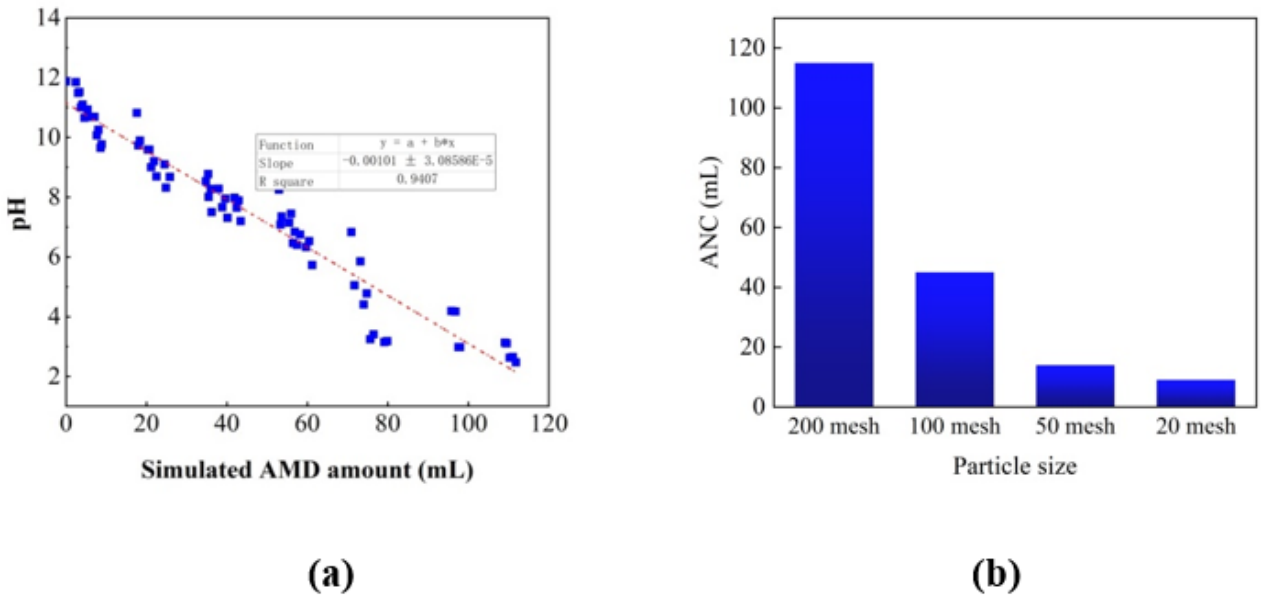


## Figure 2

ANC determination results (a) pH variations with titration of simulated AMD; (b) influence of particle sizes on the ANC of slag samples

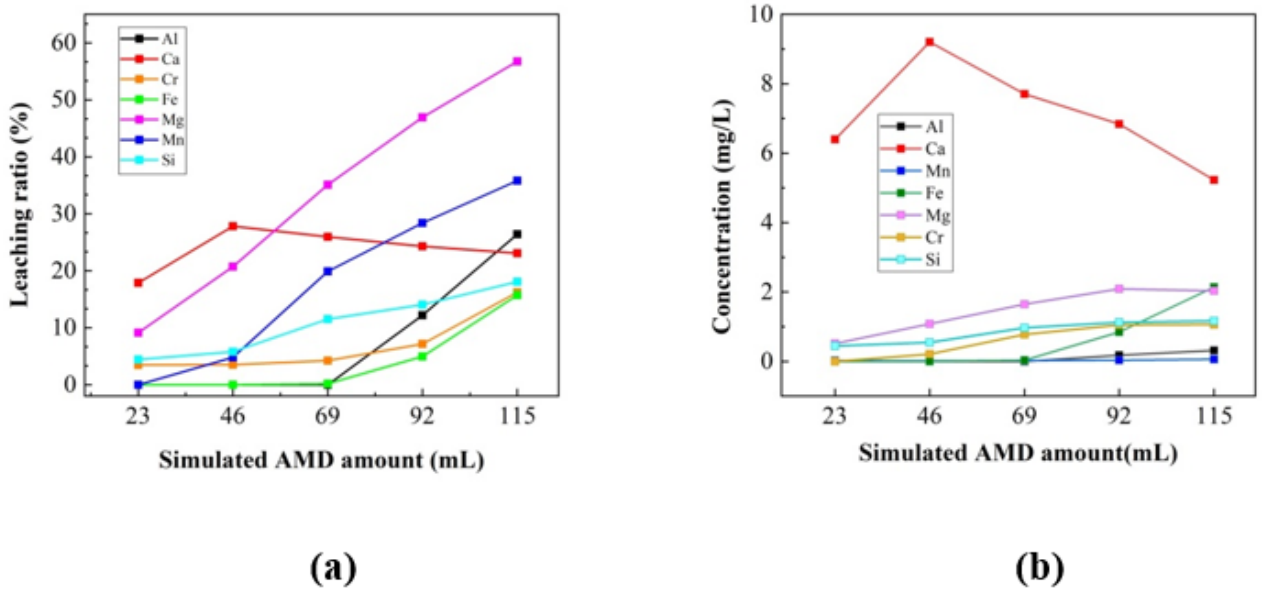


## Figure 3

Leaching behavior of slag samples in the titration process (a) Leaching ratios; (b) Leaching concentrations

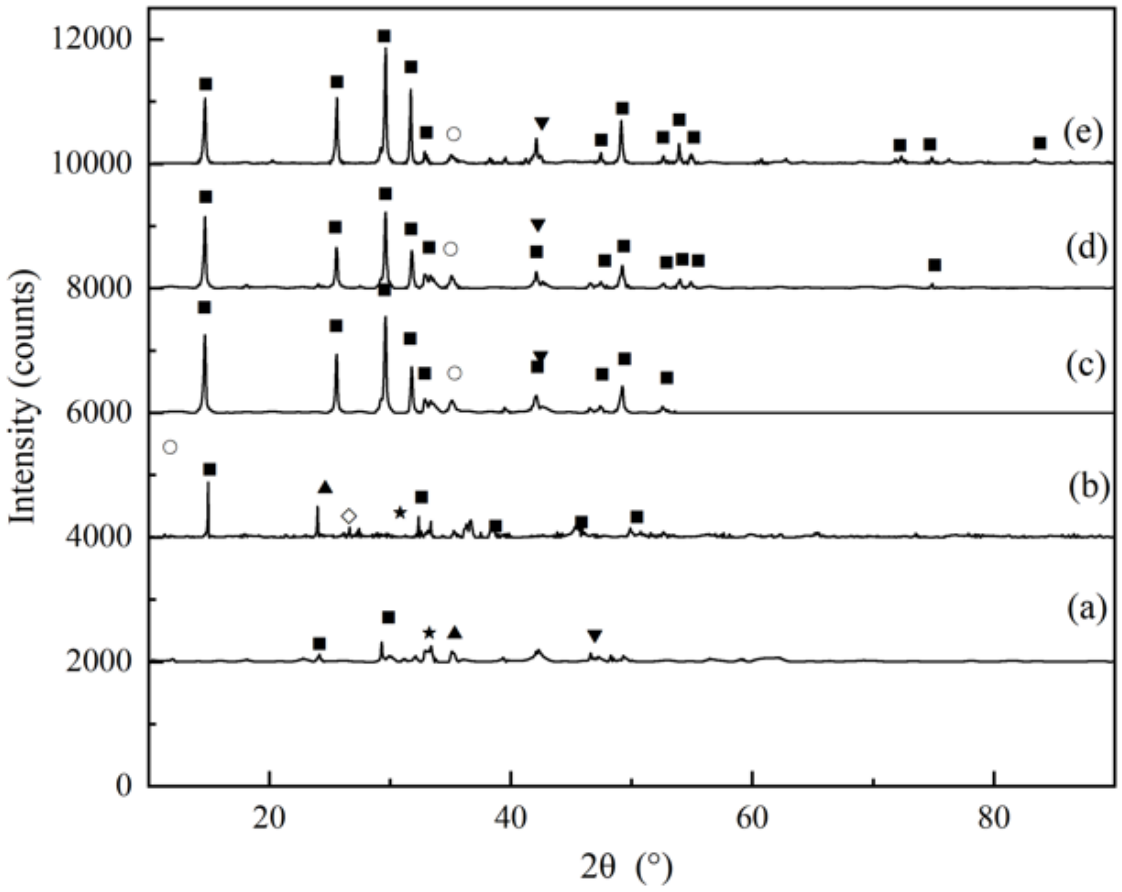


## Figure 4

XRD patterns of simulated AMD titrated slag samples (a) titrated by 23 mL simulated AMD, (b) 46 mL, (c) 72 mL, (d) 95mL, (e) 115 mL. The following compounds were identified: (■) $CaSO_4 \cdot 0.5\ H_2O$; (●) $CaFeSi_2O_6$; (▲) Mg-Al hydrotalcite; (⍰) CaO; (▼) $Ca_2SiO_4$; (⍰) RO, $(Mg, Mn, Ca)_x\ Fe_{1-x}O$;(□), $Ca_3SiO_5$

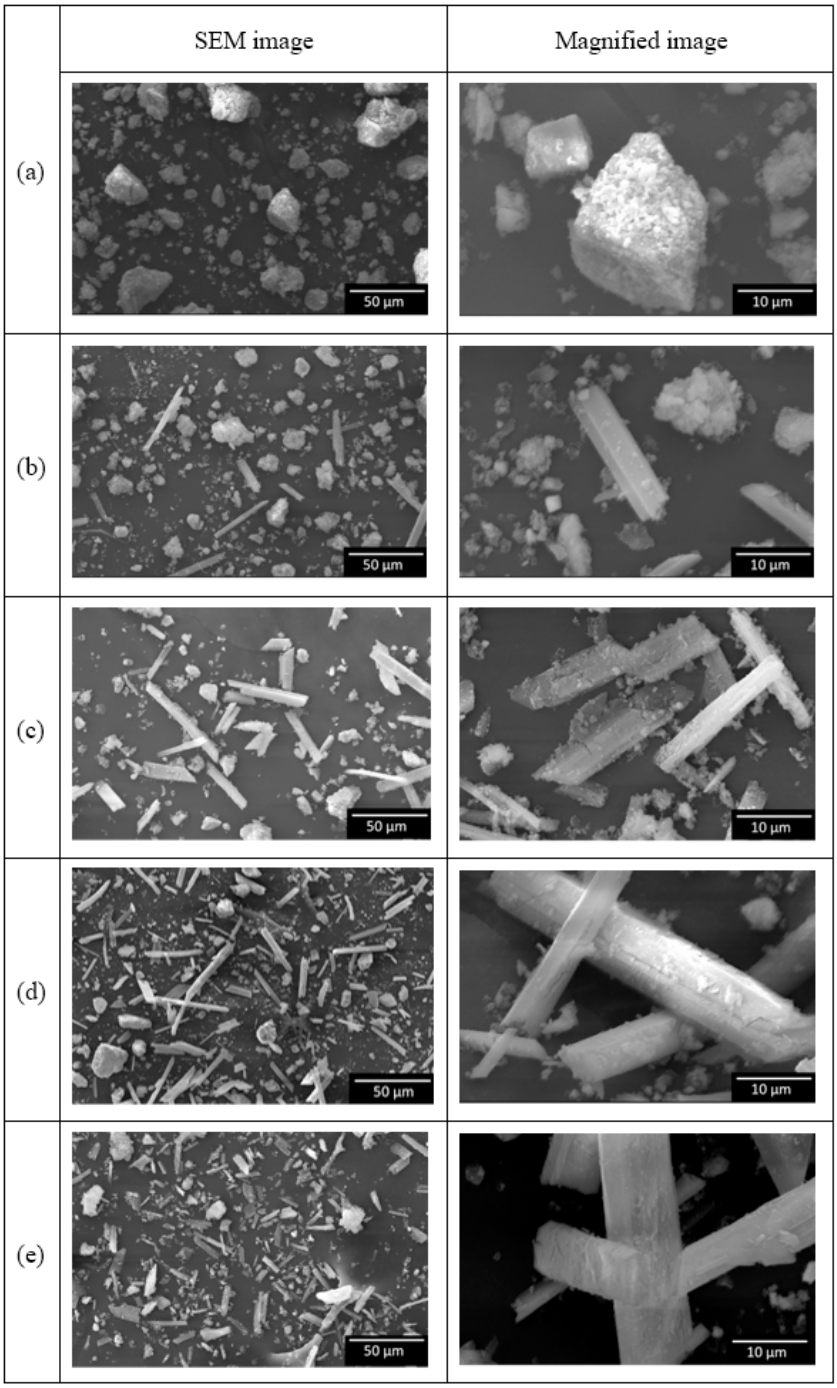


## Figure 5

**SEM images of the slag samples titrated with various simulated AMD amounts:** (a) 23ml, (b) 46ml, (c) 69ml, (d) 92 ml, and (e) 125ml.

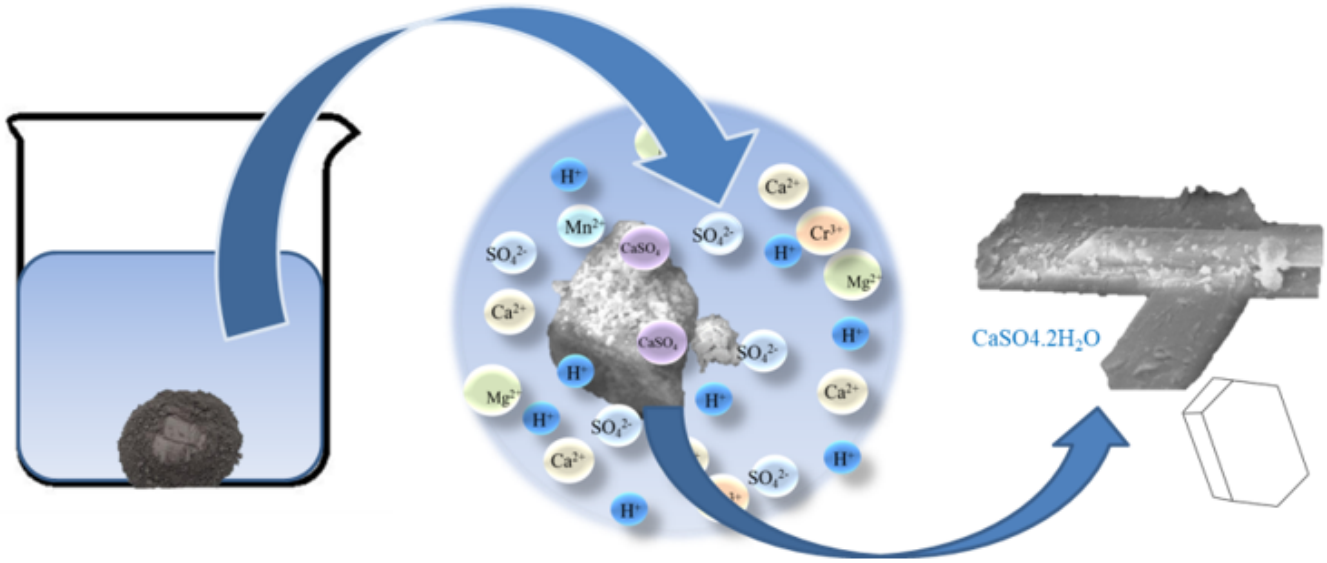


## Figure 6

Mechanism of steel slag variation process

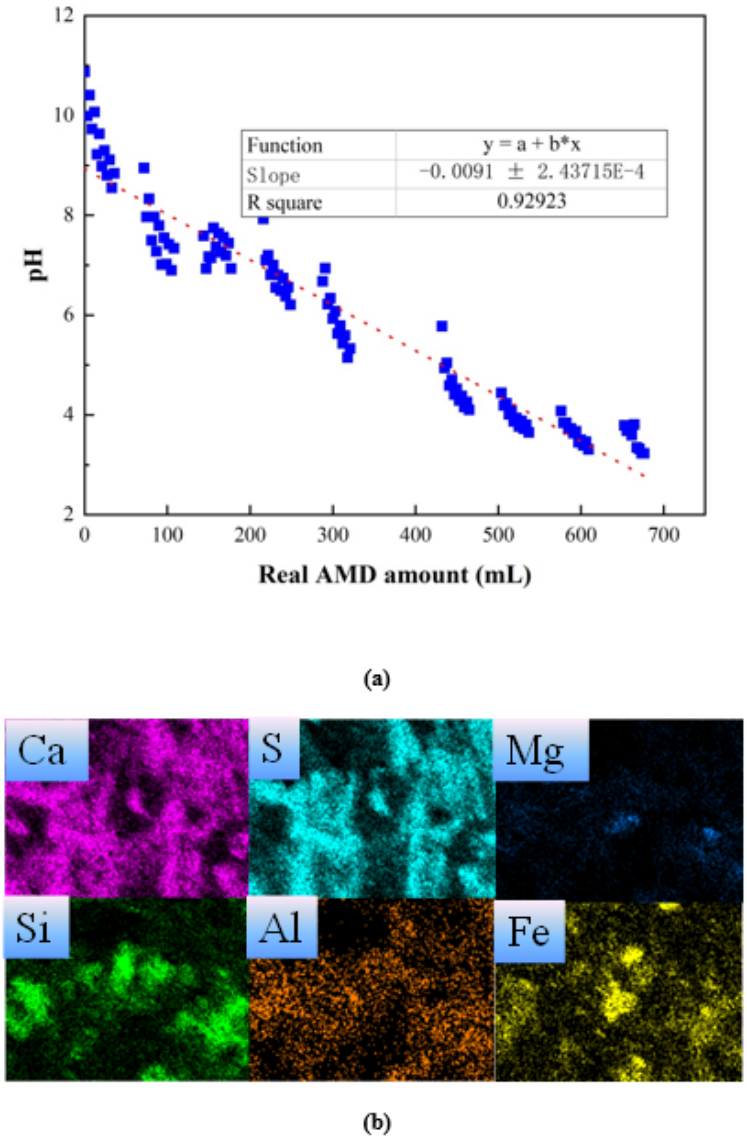


**Figure 7**

Slag ANC titrated by real AMD results (a) pH variation with the titration of real AMD (b) the elements distribution on slag surface titrated by real AMD.

## Supplementary Files

This is a list of supplementary files associated with this preprint. Click to download.

- Supplementaryfile.docx